Full-profile fitting of emission spectrum to determine transition intensity parameters of Yb^{3+}:$GdTaO_4$*

Qingli Zhang(张庆礼)[1,†], Guihua Sun(孙贵花)[1], Kaijie Ning(宁凯杰)[1], Chaoshu Shi(施朝淑)[2], Wenpeng Liu(刘文鹏)[1], Dunlu Sun(孙敦陆)[1], and Shaotang Yin(殷绍唐)[1]

[1] *The Key Laboratory of Photonic Devices and Materials, Anhui Institute of Optics and Fine Mechanics, Chinese Academy of Sciences, Hefei* 230031, *China*
[2] *Physics Department of the Science and Technology of China, Hefei* 230026, *China*

(Received 22 June 2016; revised manuscript received 28 July 2016; published online 13 October 2016)

The Judd–Ofelt theoretic transition intensity parameters A_{tp}^k of luminescence of rare-earth ions in solids are important for the quantitative analysis of luminescence. It is very difficult to determine them with emission or absorption spectra for a long time. A "full profile fitting" method to obtain A_{tp}^k in solids with its emission spectrum is proposed, in which the contribution of a radiative transition to the emission spectrum is expressed as the product of transition probability, line profile function, instrument measurement constant and transition center frequency or wavelength, and the whole experimental emission spectrum is the sum of all transitions. In this way, the emission spectrum is expressed as a function with the independent variables intensity parameters A_{tp}^k, full width at half maximum (FWHM) of profile functions, instrument measurement constant, wavelength, and the Huang–Rhys factor S if the lattice vibronic peaks in the emission spectrum should be considered. The ratios of the experimental to the calculated energy lifetimes are incorporated into the fitting function to remove the arbitrariness during fitting A_{tp}^k and other parameters. Employing this method obviates measurement of the absolute emission spectrum intensity. It also eliminates dependence upon the number of emission transition peaks. Every experiment point in emission spectra, which usually have at least hundreds of data points, is the function with variables A_{tp}^k and other parameters, so it is usually viable to determine A_{tp}^k and other parameters using a large number of experimental values. We applied this method to determine twenty-five A_{tp}^k of Yb^{3+} in $GdTaO_4$. The calculated and experiment energy lifetimes, experimental and calculated emission spectrum are very consistent, indicating that it is viable to obtain the transition intensity parameters of rare-earth ions in solids by a full profile fitting to the ions' emission spectrum. The calculated emission cross sections of Yb^{3+}:$GdTaO_4$ also indicate that the F–L formula gives larger values in the wavelength range with reabsorption.

Keywords: transition intensity, rare-earth ions, Yb^{3+}:$GdTaO_4$, luminescence

PACS: 78.55.–m, 78.60.Lc, 75.10.Dg **DOI:** 10.1088/1674-1056/25/11/117802

1. Introduction

Phosphors activated by rare-earth ions have been used widely in many fields such as displays, illumination, lasers, and so on. It is important to study the transition intensity of rare-earth in solids and aqueous solution by theory and experiments. Judd and Ofelt independently gave a quantitative description of the transition intensity in 1962.[1,2] The original idea in Judd's and Ofelt's papers is that the wavefunctions of *n*g and *n*d configuration with opposite parities are mixed into the 4f configuration by odd crystal field and the parity-forbidden rule of 4f–4f transition of electric dipole is broken down, resulting in the sharp lines of 4f–4f observed experimentally. *Ab initio* calculation has shown that the contribution from the static electric interaction is not dominant, but overlap, covalence, and polarization are also very important for the rare-earth ions in a crystal field. Hence, a more general phenomenal equation, which is very similar to that obtained by Judd and Ofelt but represents more physical effects such as overlap, covalence, and polarization, was developed by Reid *et al.* and Newman *et al.*[3–6]

Transition intensity of rare-earth ions based on the Judd–Ofelt work has been accepted and used widely to analyze the optical transition of rare-earth ions in solids, aqueous solutions, glass, and so on, which are generally applied to their absorption spectra. So far, it has been very rare to use emission spectra of rare-earth ions to fit transition intensity parameters. As pointed out by M. F. Reid, emission spectra can be particularly troublesome, since absolute measurements are difficult. It is possible to carry out fitting using relative intensities within crystal field splitting multiplets, but is not as satisfactory as using absolute intensities.[7] It will be shown in this paper that it is not feasible to determine intensity parameters reliably if no other constraints are incorporated into the fitting. Generally, for absorption measurement of solids, it is necessary to grow large, high-quality single crystal, requiring much time and money. In most cases, it is not so easy to grow single crystal whose size and quality are desirable for absorption measurement. Due to this limitation, the emission spectra of rare-earth ions in polycrystalline have rarely been investigated

*Project supported by the National Natural Science Foundation of China (Grant Nos. 51172236, 51502292, 51272254, 51102239, 61205173, and 61405206).
†Corresponding author. E-mail: zql@aiofm.ac.cn
© 2016 Chinese Physical Society and IOP Publishing Ltd

by transition intensity theory. While it is possible in some cases to calibrate the emission data by assuming that calculated magnetic dipole intensities are accurate,[5] in the great bulk of cases, the magnetic dipole transition is not so strong or is discerned difficultly, and no intensity calibration is viable.

On the other hand, integral quantities such as line strength and oscillator strength of the absorption spectrum are usually used to fit intensity parameters. The number of intensity parameters A^k_{tp} is usually large, in some cases far exceeding the number of available experimental data points, which results in fitting difficulty. This is the case when the site symmetry of rare-earth ions is very low. For example, there are twenty-five intensity parameters when a rare-earth ion is in a C_2 site symmetry. If the transition intensity of Yb^{3+} in C_2 was to be fitted, at best only three absorption peaks corresponding to three integral absorption quantities such as line strength or oscillator strength are available, far less than the number of intensity parameters to be determined.

In order to overcome these difficulties of fitting the transition intensity of rare-earth ions to emission or absorption spectra, we propose a "full profile method." As a practical example, the intensity parameters and Huang–Rhys factors were fitted to the emission spectrum of Yb:$GdTaO_4$, a promising ultra-short pulse laser medium, at 8 K. Also, some problems related to Yb^{3+} in solids are discussed. The results of fitting to the emission spectrum of Yb^{3+}:$GdTaO_4$ indicate that the full-profile method is a viable way to determine transition intensity parameters through a powder crystalline emission spectrum, and the difficulty that the number of the intensity integral quantities of the spectrum is smaller than that of the intensity parameters and other relative parameters is overcome.

2. Full-profile fitting emission spectrum to determine transition intensity parameters

2.1. Basic aspect for transition intensity

Considering an emission band from the transition between the initial energy levels E_I with an initial population number N_I and final energy levels E_F, whose initial and final wavefunctions are $|Ii_\alpha\rangle$ $(\alpha = 1,\ldots,g_i)$ and $|Ff_\beta\rangle$ $(\beta = 1,\ldots,g_f)$, where g_i and g_f are the degeneration of energy levels E_I and E_F, respectively, the electronic and magnetic dipole transition line strength $S^{\rm ed}_{IF}$ and $S^{\rm md}_{IF}$ from E_I to E_F can be calculated by

$$\mathcal{S}^{\rm ed}_{IF,q} = \sum_{\alpha,\beta}\left|\langle Ii_\alpha|D^1_q|Ff_\beta\rangle\right|^2 = \sum_{\alpha,\beta}\left|\left(M^{\rm ed}_{i_\alpha,f_\beta}\right)_q\right|^2, \quad (1)$$

$$\mathcal{S}^{\rm md}_{IF,q} = \sum_{\alpha,\beta}\left|\langle Ii_\alpha|(\boldsymbol{L}+2\boldsymbol{S})_q|Ff_\beta\rangle\right|^2 = \sum_{\alpha,\beta}\left|\left(M^{\rm md}_{i_\alpha,f_\beta}\right)_q\right|^2, \quad (2)$$

where $\boldsymbol{L}$ and $\boldsymbol{S}$ are orbital and spin angular momentum operators, $\boldsymbol{L}+2\boldsymbol{S} = \boldsymbol{J}+\boldsymbol{S}$, where $\boldsymbol{J}$ is the spin–orbital coupling angular momentum operator, both $\boldsymbol{J}$ and $\boldsymbol{S}$ are one-rank spherical tensors, whose matrix elements in the space spanned by the base vectors $|aSLJM\rangle$ (S, L, J are spin, orbital, spin–orbital coupling angular momentums, respectively, and M is J angular momentum component) can be computed by the Wigner–Echart theorem and the general tensor matrix element formula, such as Eqs. (2–27) and (3–37) in Ref. [8].

The non-polarized luminescence line strength for powder polycrystalline should be averaged as

$$\mathcal{S}^{\rm ed}_{IF} = \frac{1}{3}(S^{\rm ed}_{IF,1}+S^{\rm ed}_{IF,0}+S^{\rm ed}_{IF,1}), \quad (3)$$

$$\mathcal{S}^{\rm md}_{IF} = \frac{1}{3}(S^{\rm md}_{IF,1}+S^{\rm md}_{IF,0}+S^{\rm md}_{IF,1}). \quad (4)$$

According to Judd–Ofelt parameterization, the matrix element of electric dipole transition is

$$\langle Ii_\alpha|D^1_q|Ff_\beta\rangle = \sum_{\text{even } k,\text{odd } t} D^k_{tp,q}\cdot A^k_{tp}, \quad (5)$$

where

$$D^k_{tp,q} = \langle Ii_\alpha|U^k_{p+q}|Ff_\beta\rangle\,(-1)^{p+q}\,[k]\begin{pmatrix}1 & k & t\\ q & -(p+q) & q\end{pmatrix}, \quad (6)$$

$$A^k_{tp} = A^p_t\,\Xi(t,k), \quad (7)$$

$$\Xi(t,k) = \sum_{n'l'} K\left(t,k,l,l'\right)\overline{r^{t+1}}(n,l,n',l'), \quad (8)$$

$$K\left(t,k,l,l'\right) = 2\,[l]\,[l'](-1)^{l+l'}\begin{Bmatrix}1 & k & t\\ l & l' & l\end{Bmatrix}\begin{Bmatrix}l & 1 & l'\\ 0 & 0 & 0\end{Bmatrix} \times\begin{pmatrix}l' & t & l\\ 0 & 0 & 0\end{pmatrix}, \quad (9)$$

$$\overline{r^{t+1}}\left(n,l,n',l'\right) = \langle nl\,|r|\,n'l'\rangle\langle n'l'\,|r^t|\,nl\rangle/\Delta(n'l'), \quad (10)$$

where D^1_q is the electric dipole operator, nl is 4f for the rear-earth ion, $n'l'$ is the excited configuration with opposite parity to the 4f configuration, and $\Delta(n'l')$ is the energy separation between the 4f and $n'l'$ configurations. It is usually very difficult to compute the value of $\overline{r^{t+1}}\,(n,l,n',l')$, because it is necessary to know the detailed wavefunction $|n'l'\rangle$. Generally, t is odd, $t = 1, 3, 5, 7$, and t is decided by the condition that $\sum_{t,p} A^p_t C^t_p$ is an identity representation under the site symmetry operation. While, k is even and decided by triangle-relation $\Delta(1kt)$ in the three-j expression $\begin{pmatrix}1 & k & t\\ q & -(p+q) & q\end{pmatrix}$ of Eq. (6), i.e., $k = t\pm 1$.

The spontaneous emission transition probability A_{IF} can be calculated with the values $\langle Ii_\alpha|D^1_q|Ff_\beta\rangle$.

2.2. Full profile fitting determination of transition intensity parameters

2.2.1. First, all of the emission spectrum data points can be expressed as a function with the independent variables A^k_{tp} and other parameters

Using the spontaneous transition probability $A_{IF}\left(A^k_{tp}\right)$, the photoluminescence transition intensity $\mathcal{I}_{IF}$ from E_I to E_F can be expressed as

$$\mathcal{I}_{IF} = \sigma A_{IF}\left(A^k_{tp}\right)N_I h\nu_{IF}, \quad (11)$$

where h is the Plank constant, ν_{IF} is the emission frequency from the initial state I to the final state F, its value is $\nu_{IF} = |E_I - E_F|/h$ and the corresponding emission wavelength $\lambda_{IF} = hc/|E_I - E_F|n$, c is the light velocity in vacuum, and σ is a constant that depends on the measurement conditions, which we call an instrumental constant. The absolute intensity $A_{IF}\left(A^k_{tp}\right) N_I h\nu_{IF}$ in J/m^3·s is photon energy emitted from the phosphor sample per unit volume per second, and generally is converted into electric current signal by a photoelectric detector such as a photomultiplier tube, whose converted coefficient is σ. It is too troublesome to demarcate σ due to the circumstances, which depend not only on excitation light intensity, phosphor position, pose and excitation area, activator concentration, but also on the sensor sensitivity and so on, so many effects should be considered that it is infeasible. On the other hand, it is unnecessary for an overwhelming majority of spectra measurements because the relative spectral intensity is enough in many cases. So it is very difficult to determine the absolute intensity $A_{IF}\left(A^k_{tp}\right)N_I h\nu_{IF}$ due to the unknown quantity σ. Meanwhile, when the intensity contribution from magnetic dipole transition, which is usually weaker by a few of orders than that of electric dipole transition, is omitted, if A^k_{tp} is multiplied by an arbitrary constant s, then

$$\mathcal{I}_{IF} = \sigma A_{IF}(sA^k_{tp})N_I h\nu_{IF} = s^2\sigma A_{IF}(A^k_{tp})N_I h\nu_{IF}. \quad (12a)$$

The values of σ and $s^2\sigma$ cannot be discerned experimentally, indicating that the uncertainty of the instrumental constant results in the uncertainty of A^k_{tp}. Subsequently, it is difficult to directly determine the transition intensity parameters A^k_{tp} with the luminescence spectrum.

Equation (12a) can be expressed as

$$\mathcal{I}_{IF} = \sigma_I A_{IF}(A^k_{tp})\nu_{IF}, \quad (12b)$$

if σ and $N_I h$ are combined as a quantity, that is

$$\sigma_I = \sigma N_I h. \quad (13a)$$

It is obvious that σ_I depends not only on the instrumental constant σ but also on the population N_I in the initial state I. It is a great problem for spectroscopy to know the excited state population N_I, which further indicates that it is difficult to obtain the absolute fluorescence intensity $N_I A_{IF}\left(A^k_{tp}\right)\nu_{IF}$, so in the full profile fitting, σ_I is fitted as a variable. The magnitude of ν_{IF} is about 10^{14}–10^{15} s^{-1} for the fluorescence in the wavelength range 100 mm–1000 nm, A_{IF} is about 1–10^3 s^{-1} for rare-earth ions, $\mathcal{I}_{IF}$ is about 10^{-1} for a normalized emission spectrum, so the magnitude of σ_I is about 10^{-19}–10^{-14} s. In order to keep all of the fitted parameters nearly on the same order, σ_I is written as

$$\sigma_I = C\sigma'_I, \quad (13b)$$

where C is an adjustable parameter manually, usually on the order 10^{-19}–10^{-14} s, and σ'_I is a parameter fitted by a computational routine.

Assuming that the transition line profile function from E_I to E_F is $\phi_{IF}(\lambda, \lambda_{IF}, w_{IF})$ against λ with the full width at half maximum (FWHM) w_{IF} and peak center λ_{IF}, $\phi_{IF}(\lambda, \lambda_{IF}, w_{IF})$ is normalized by

$$\int \phi_{IF}(\lambda, \lambda_{IF}, w_{IF})\,\mathrm{d}\lambda = 1, \quad (14)$$

where $\phi_{IF}(\lambda, \lambda_{IF}, w_{IF})$ may be a Lorenz, Gauss or Voigt function, and so on. If the line profile function is a Voigt function, w should be w_{L} and w_{G}, which are the FWHM of the Lorentz and Gauss components. Using the line profile function $\phi_{IF}(\lambda, \lambda_{IF}, w)$, the transition intensity $\mathcal{I}_{IF}(\lambda)$ from E_I to E_F in the whole measurement spectral range can be expressed as

$$\mathcal{I}_{IF}(\lambda) = \mathcal{I}_{IF}\phi_{IF}(\lambda, \lambda_{IF}, w_{IF}). \quad (15)$$

The total intensity of a spectrum from all transitions can be expressed as

$$\begin{aligned}\mathcal{I}(\lambda) &\equiv \mathcal{I}\left(\lambda, A^k_{tp}, \lambda_{IF}, w\right) = \sum\nolimits_{I,F}\mathcal{I}_{IF}(\lambda) \\ &= \sum\nolimits_{I,F}\sigma_I A_{IF}(A^k_{tp})\phi_{IF}(\lambda, \lambda_{IF}, w)\nu_{IF}. \end{aligned} \quad (16)$$

If the integral intensity of a spectral band from E_{I_0} to E_{F_0} is called $\mathcal{I}_0$, the relative emission intensity can be obtained as

$$\begin{aligned}\mathcal{I}'(\lambda) &\equiv \mathcal{I}'\left(\lambda, A^k_{tp}, \lambda_{IF}, w, \mathcal{R}_{IF}\right) = \frac{\mathcal{I}(\lambda)}{\mathcal{I}_0} \\ &= \sum\nolimits_{I,F}\mathcal{R}_{IF}\frac{\nu_{IF}A_{IF}(A^k_{tp})}{\nu_{I_0F_0}A_{I_0F_0}(A^k_{tp})}\phi_{IF}(\lambda, \lambda_{IF}, w), \quad (17a) \\ \mathcal{R}_{IF} &= \frac{N_I}{N_{I_0}}. \quad (17b)\end{aligned}$$

If a spectrum is only from one initial state, $\mathcal{R}_{IF} = 1$, equation (17a) can be simplified as

$$\mathcal{I}'(\lambda) = \sum\nolimits_{I,F}\frac{\nu_{IF}A_{IF}(A^k_{tp})}{\nu_{I_0F_0}A_{I_0F_0}(A^k_{tp})}\phi_{IF}(\lambda, \lambda_{IF}, w). \quad (17c)$$

Now every data point $\mathcal{I}(\lambda)$ in a spectrum is expressed as a function with the independent variables A^k_{tp}, $\mathcal{R}_{IF}$ or σ_I, w_{IF} and λ_{IF}, by Eqs. (16)–(17c). λ_{IF} can be directly obtained through line peaks. Usually a spectrum is composed of hundreds or thousands of experimental data points $\mathcal{I}_{\mathrm{obs}}(\lambda)$ corresponding to the calculated point $\mathcal{I}(\lambda)$, so it is possible to determine the transition intensity parameters A^k_{tp}, w_{IF} and $\mathcal{R}_{IF}$, as well as the Huang–Rhys factor S (described later), which are written in a variable vector $\boldsymbol{x}$ for convenience later. The $\mathcal{I}(\lambda)$ is expressed as the following general form $\mathcal{I}(\lambda, \boldsymbol{x})$, i.e.,

$$\mathcal{I}(\lambda) \equiv \mathcal{I}(\lambda, \boldsymbol{x}). \quad (18)$$

2.2.2. Second, in order to remove arbitrariness of the parameters, a quantity associated with the ratio of the experimental to calculated fluorescence decaytime is incorporated into the fitting

According to Eqs. (17a)–(17c), although $\mathcal{I}'(\lambda)$ is independent of the instrumental constant σ when all of the transitions are from the same initial state, it keeps uncertainty. If the magnetic dipole contribution to transition intensity is omitted, let all of A_{tp}^k be multiplied by an arbitrary constant s,

$$\begin{aligned}\mathcal{I}'(\lambda,\boldsymbol{x}) &= \sum_{I,F}\frac{\nu_{IF}A_{IF}(sA_{tp}^k)}{\nu_{I_0F_0}A_{I_0F_0}(sA_{tp}^k)}\phi_{IF}(\lambda,\lambda_{IF},w)\\ &= \sum_{I,F}\frac{\nu_{IF}A_{IF}(A_{tp}^k)}{\nu_{I_0F_0}A_{I_0F_0}(A_{tp}^k)}\phi_{IF}(\lambda,\lambda_{IF},w).\end{aligned}$$

That is, A_{tp}^k multiplied by an arbitrary constant s would not change the relative intensity $\mathcal{I}'(\lambda,\boldsymbol{x})$. The uncertainty has not been removed although the instrumental constant σ has been removed from the relative intensities.

On the other hand, if all A_{tp}^k are multiplied by s, every fluorescence decaytime τ_j changes to τ_j/s^2 when the magnetic dipole transitions are omitted, so the fluorescence decaytime can be used as an "emendation standard" for A_{tp}^k to remove arbitrariness from the determination, so a quantity $y(\boldsymbol{x})$, which depends on the fluorescence decaytime, can be introduced to fit A_{tp}^k and other parameters, is expressed as

$$\begin{aligned}y(\boldsymbol{x}) &= \frac{1}{2}\sum_{j=1}^{M}\left(1-\frac{\tau_j^{\rm obs}}{\tau_j^{\rm cal}(\boldsymbol{x})}\right)^2\\ &= \frac{1}{2}\sum_{j=1}^{M}\left(1-\tau_j^{\rm obs}\sum_F A_{j_IF}(\boldsymbol{x})\right)^2,\end{aligned}\tag{19}$$

where $\tau_j^{\rm obs}$ and $\tau_j^{\rm cal}(\boldsymbol{x})$ are the observed and calculated energy lifetimes of the j_I-th crystal field energy levels, respectively. It can be seen that if $\tau_j^{\rm cal}(\boldsymbol{x})\gg\tau_j^{\rm obs}$, $\tau_j^{\rm obs}/\tau_j^{\rm cal}(\boldsymbol{x})\to 0$, then $y(\boldsymbol{x})\to M/2$, if $\tau_j^{\rm cal}(\boldsymbol{x})\ll\tau_j^{\rm obs}$, $\tau_j^{\rm obs}/\tau_j^{\rm cal}(\boldsymbol{x})\to\infty$, then $y(\boldsymbol{x})\to\infty$, so the minimal value of $y(\boldsymbol{x})$ is zero only when $\tau_j^{\rm obs}=\tau_j^{\rm cal}(\boldsymbol{x})$. The observed $\tau_j^{\rm obs}$ is constant, and $1/\tau_j^{\rm cal}$ is proportional to $\sum_F A_{j_IF}(\boldsymbol{x})$, so A_{tp}^k cannot be scaled arbitrarily, due to the minimum limit of Eq. (19) and the arbitrariness of A_{tp}^k can be removed by incorporating $y(\boldsymbol{x})$ into the optical transition intensity fitting.

To a great extent, the reliability of determining the parameters depends on the degree of consistency between $\tau_j^{\rm obs}$ and $\tau_j^{\rm cal}$, which implies the follows.

1) $\tau_j^{\rm obs}$ is mainly from the radiative transition, and the nonradiative contribution can be omitted, and $\tau_j^{\rm obs}$ can generally be written as

$$\tau_j^{\rm obs}=\frac{1}{\sum_F A_{j_IF}(\boldsymbol{x})+W},$$

where W is nonradiative transition probability. Let $W=\delta\sum_F A_{j_IF}(\boldsymbol{x})$,

$$\tau_j^{\rm obs}=\frac{1}{\delta+1}\frac{1}{\sum_F A_{j_IF}(\boldsymbol{x})}=\frac{1}{\delta+1}\tau_j^{\rm cal}(\boldsymbol{x}),$$

and the relative measurement error $\Delta(\tau_j^{\rm cal}(\boldsymbol{x}))$ of $\tau_j^{\rm cal}$ is $(\tau_j^{\rm obs}-\tau_j^{\rm cal}(\boldsymbol{x}))/\tau_j^{\rm cal}(\boldsymbol{x})=-\delta/(\delta+1)$. Further assuming that $\delta+1$ is all ascribed to A_{tp}^k, then A_{tp}^k with error should be $\sqrt{\delta+1}A_{tp}^k$, and the relative error $\Delta(A_{tp}^k)$ for A_{tp}^k is $(\sqrt{\delta+1}-1)$. As an example, let δ =0.1, $\Delta(\tau_j^{\rm cal}(\boldsymbol{x}))=9.1\%$, $\Delta(A_{tp}^k)=4.8\%$, if $\delta=0.2$, $\Delta(\tau_j^{\rm cal}(\boldsymbol{x}))=16.7\%$, $\Delta(A_{tp}^k)=9.5\%$. The nonradiative transition ratio for many optical transitions of rare-earth ions at low temperature is less than 0.1, so the error of the determined A_{tp}^k that is caused by nonradiative transition is small.

2) To what degree does the calculated $\tau_j^{\rm cal}$ trend to $\tau_j^{\rm cal}$. The $\tau_j^{\rm cal}$ can be adjusted to be very close to $\tau_j^{\rm obs}$ in practice, with a difference that is usually less than 5%. As the above analysis, $\delta/(\delta+1)<0.05$, then $\delta<0.05$, $\Delta(A_{tp}^k)<2.6\%$, which is very small and can be omitted.

2.2.3. Third, the least-square fitting with a general iteration method is performed to solve the transition intensity and other parameters

In order to solve for variable $\boldsymbol{x}$, least-squares fitting to the emission spectrum should be performed, which is generally to minimize the following difference value φ including $y(\boldsymbol{x})$,

$$\begin{aligned}\varphi(\boldsymbol{x}) &= \frac{1}{2}\sum_{\lambda}(\mathcal{I}_{\rm obs}(\lambda)-\mathcal{I}(\lambda,\boldsymbol{x}))^2+y(\boldsymbol{x})\\ &= \frac{1}{2}\sum_{\lambda}(\mathcal{I}_{\rm obs}(\lambda)-I(\lambda,\boldsymbol{x}))^2\\ &\quad+\frac{1}{2}\sum_{j=1}^{M}\left(1-\tau_j^{\rm obs}\sum_F A_{j_IF}(\boldsymbol{x})\right)^2.\end{aligned}\tag{20}$$

The recorded spectral intensity is a series of discrete wavelength and intensity values $(\lambda_1, I(\lambda_1))$, $(\lambda_2, I(\lambda_2))$, …, $(\lambda_N, I(\lambda_N))$, so equation (20) can be written as

$$\begin{aligned}\varphi(\boldsymbol{x}) &= \frac{1}{2}\boldsymbol{f}^{\rm T}(\boldsymbol{x})\boldsymbol{f}(\boldsymbol{x})=\frac{1}{2}\sum_{i}(\mathcal{I}_{\rm obs}(\lambda_i)-I(\lambda_i,\boldsymbol{x}))^2\\ &\quad+\frac{1}{2}\sum_{j=1}^{M}\left(1-\tau_j^{\rm obs}\sum_F A_{j_IF}(\boldsymbol{x})\right)^2,\end{aligned}\tag{21}$$

where

$$\boldsymbol{f}(\boldsymbol{x})=\begin{bmatrix}f_1(\boldsymbol{x})\\ f_2(\boldsymbol{x})\\ \vdots\\ f_N(\boldsymbol{x})\\ f_{N+1}(\boldsymbol{x})\\ \vdots\\ f_{N+M}(\boldsymbol{x})\end{bmatrix}=\begin{bmatrix}\mathcal{I}_{\rm obs}(\lambda_1)-\mathcal{I}^{(\lambda_1,\boldsymbol{x})}\\ \mathcal{I}_{\rm obs}(\lambda_2)-\mathcal{I}^{(\lambda_2,\boldsymbol{x})}\\ \vdots\\ \mathcal{I}_{\rm obs}(\lambda_N)-\mathcal{I}^{(\lambda_N,\boldsymbol{x})}\\ 1-\dfrac{\tau_1^{\rm obs}}{\tau_1^{\rm cal}(\boldsymbol{x})}\\ \vdots\\ 1-\dfrac{\tau_M^{\rm obs}}{\tau_M^{\rm cal}(\boldsymbol{x})}\end{bmatrix}.\tag{22}$$

The minimum of the normal equation of Eq. (20) can be obtained by

$$\nabla\varphi(\boldsymbol{x}) = D\boldsymbol{f}^{\mathrm{T}}(\boldsymbol{x})\,\boldsymbol{f}(\boldsymbol{x}) = 0, \tag{23}$$

where

$$D\boldsymbol{f}^{\mathrm{T}}(\boldsymbol{x}) = \begin{bmatrix} \dfrac{\partial f_1}{\partial x_1} & \cdots & \dfrac{\partial f_{N+M}}{\partial x_1} \\ \vdots & \vdots & \vdots \\ \dfrac{\partial f_1}{\partial x_n} & \cdots & \dfrac{\partial f_{N+M}}{\partial x_n} \end{bmatrix}, \tag{24}$$

and n is the variable component number of the variables A^k_{tp}, w_{IF} and $\mathcal{R}_{IF}$, as well as that of the Huang–Rhys factor S if necessary.

The $\boldsymbol{x}$ can be obtained by solving Eq. (23), which is a nonlinear equation system and can be solved by the Levenberg–Marquardt method, whose iteration formula is given by

$$\begin{aligned} \boldsymbol{x}^{k+1} = \boldsymbol{x}^k - &\left[D\boldsymbol{f}^{\mathrm{T}}\left(\boldsymbol{x}^k\right) D\boldsymbol{f}\left(\boldsymbol{x}^k\right) + \mu_k \boldsymbol{I}\right]^{-1} \\ &\times \left[D\boldsymbol{f}^{\mathrm{T}}\left(\boldsymbol{x}^k\right) \boldsymbol{f}\left(\boldsymbol{x}^k\right)\right], \\ &(k = 0, 1, \ldots,), \end{aligned} \tag{25}$$

where k stands for the k-th iteration, $\boldsymbol{x}^k$ is the value at the k-th iteration, μ_k is damping factor at the k-th iteration, and $\boldsymbol{I}$ is unit matrix.

3. Full-profile fitting the emission spectrum of Yb^{3+}:$GdTaO_4$ to determine its spectral intensity parameters and Huang–Rhys factor

3.1. Low temperature photoluminescence spectrum of Yb^{3+}:$GdTaO_4$

The (5 at.%) Yb^{3+}:$GdTaO_4$ was prepared by a high temperature solid state reaction method. The raw materials were Yb_2O_3, Gd_2O_3, and Ta_2O_5 with purity 99.999%. They were weighted according to the constitute ratio of $Yb_{0.05}Gd_{0.95}TaO_4$, mixed and ground thoroughly in an agate mortar by an agate pestle. The mixtures were calcined at 1500 degree Celsius for 72 h. After the samples were cooled down to room temperature, they were thoroughly re-ground as polycrystalline powder and used as photoluminescence measurement samples. The x-ray diffraction indicates that it was M-Yb^{3+}:$GdTaO_4$ with space group $I12/a1$ (No.15),[9] and its structure was refined by GSAS using the structure data of M-$GdTaO_4$ as the initial parameters. The obtained structure data of M-Yb^{3+}:$GdTaO_4$ was used to calculate the structural data needed by superpostion mode.

The photoluminescence spectra of (5 at.%) Yb:$GdTaO_4$ at 8 K were measured with Fluorolog-3-Tau made by JOBIN YVON. Its excitation and emission spectra are shown in Figs. 1 and 2. Its excitation spectrum has relatively strong excitation peaks at 927.3 nm, 955.5 nm, and 971.8 nm, which should be from the electron state transitions of Yb^{3+}. The obvious vibronic peaks at about 930.5 nm, 934.5 nm, 936.7 nm, 943.5 nm, 947.0 nm, 950.1 nm, and 961.6 nm are also observed in its excitation spectrum. Its emission spectrum (show in Fig. 2) has four obvious peaks at 972.8 nm, 1000.3 nm, 1013.9 nm, and 1033.8 nm, which should be from the electron state transition of Yb^{3+}, and the peak at 1009.5 should be the vibronic peak of 1000.3 nm, resulting from the lattice relaxation, which will be accounted for in a later calculation. The excitation peak at 971.8 nm and emission peak at 972.8 nm should be from the transition between the lowest Stark levels of $^2F_{5/2}$ and $^2F_{7/2}$ of Yb^{3+}, according to which the phonon energy can be evaluated as 5.3 cm^{-1}. Based on these, it is assumed that the electron excitation energy incorporates a phonon of 5.3 cm^{-1}, and the electron emission energy releases a phonon of 5.3 cm^{-1} relative to a zero-line transition to calculate the crystal field splitting of Yb^{3+} in Yb^{3+}:$GdTaO_4$. The obtained crystal-field splitting of (5 at.%)Yb^{3+}:$GdTaO_4$ is shown as

$^2F_{5/2}$: 10779 cm^{-1}, 10460 cm^{-1}, 10285 cm^{-1};

$^2F_{7/2}$: 0 cm^{-1}, 283 cm^{-1}, 417 cm^{-1}, 607 cm^{-1}.

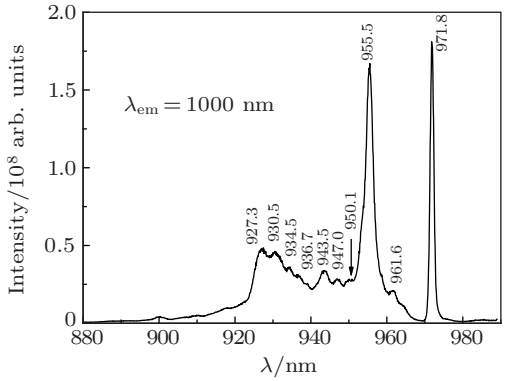


Fig. 1. The excitation spectrum of Yb^{3+}:$GdTaO_4$ with the emission wavelength of 1000 nm.

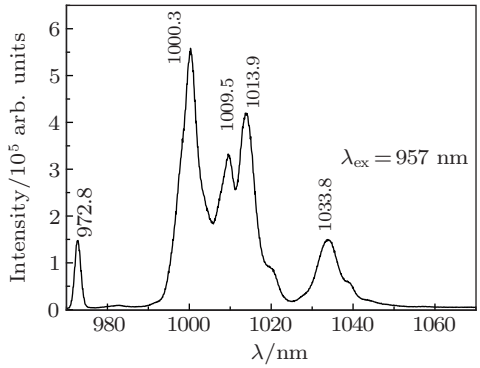


Fig. 2. The emission spectrum of Yb^{3+}:$GdTaO_4$ with the excitation wavelength 957 nm.

3.2. Vibronic peak fitting

Some obvious vibronic peaks can be observed in the photoluminescence spectrum of Yb^{3+}:$GdTaO_4$ at low temperature and the lattice relaxation during optical emission cannot be omitted. Single frequency approximation[10] was adopted to describe the lattice relaxation during emission. If p_{IF} phonons with frequency Δ_{IF} and Huang–Rhys factor S_{IF} are released during de-excitation of an electron, the matrix element M_{i_α,f_β} in Eqs. (1) and (2) is turned into $M_{\alpha,\beta}{}'$,

$$\left|M'_{i_\alpha,f_\beta}\right|^2 = \left|M_{i_\alpha,f_\beta}\right|^2 \left(\frac{\bar{n}+1}{\bar{n}}\right)^{\frac{p_{IF}}{2}} \times \mathrm{e}^{-S_{IF}(2\bar{n}+1)} \mathrm{I}_{p_{IF}}(2S_{IF}\sqrt{\bar{n}(\bar{n}+1)}), \quad (26)$$

where

$$\bar{n} = \frac{1}{\mathrm{e}^{h\Delta_{IF}/k_\mathrm{B}T}-1}, \quad (27)$$

where k_B is the Boltzmann constant, and T sample temperature; correspondingly, the emission line frequency center is $\nu'_{IF} = \nu_{IF} - \Delta_{IF}$. It can be seen that the matrix element for a zero-line thus becomes

$$|M'_{i_\alpha,f_\beta}|^2 = |M_{i_\alpha,f_\beta}|^2 \mathrm{e}^{-S_{IF}(2\bar{n}+1)} \mathrm{I}_0(2S_{IF}\sqrt{\bar{n}(\bar{n}+1)}), \quad (28)$$

where $\mathrm{I}_p(z)$ is the modified Bessel function with variable z, and its integral formula is

$$\mathrm{I}_p(z) = \frac{\left(\frac{z}{2}\right)^p}{\Gamma(p+\frac{1}{2})\Gamma(\frac{1}{2})} \int_{-1}^{1} \left(1-t^2\right)^{p-\frac{1}{2}} \mathrm{e}^{-zt}\,\mathrm{d}t \times \left(\mathrm{Re}\,p > -\frac{1}{2}\right), \quad (29)$$

where Γ is gamma function. Equation (29) can be calculated by Gauss–Legendre quadrature. The quadrature nodes can be calculated[11] or obtained from some mathematics handbooks.

3.3. Full-profile fitting the emission spectrum of Yb^{3+}:$GdTaO_4$

3.3.1. Initial parameters estimation of A^k_{tp}

The wavefunctions, $|Ii_\alpha\rangle$ and $|Ff_\beta\rangle$ mentioned previously, calculated by the superposition model parameters in Ref. [12], were used to calculate spectral transition intensity. The initial parameters A^t_p were evaluated by the point charge model in the international system of units with

$$A^t_p = \frac{1}{4\pi\varepsilon_0} \sum_L \frac{Z_j e^2}{R_L^{t+1}} C^{t*}_p(\Theta_L,\Phi_L), \quad (30a)$$

$$C^{t*}_p(\Theta_L,\Phi_L) = \sqrt{\left(\frac{4\pi}{2t+1}\right)} Y^{t*}_p(\Theta_L,\Phi_L), \quad (30b)$$

where ε_0 is the dielectric constant in vacuum, e is the charge of an electron, Z_L is the charge number of the L-th ligand, R_L is the distance between the central ion and the L-th ligand, Y^k_q is the spherical harmonic function, * stands for the complex conjugate operation, and Θ_L and Φ_L are angular coordinates of the L-th ligand. The dimension of A^t_p is energy/L^t.

Another quantity to be evaluated is $\overline{r^{t+1}}(n,l,n',l')$ in $\Xi(t,k)$, whose dimension is L^{k+1}/energy. According to Eq. (8),

$$\Xi(t,k) = K(t,k,\mathrm{f},\mathrm{d})\,\overline{r^{t+1}}(4,\mathrm{f},5,\mathrm{d}) + K(t,k,\mathrm{f},\mathrm{g}) \sum_{n'} \overline{r^{t+1}}(4,\mathrm{f},n',\mathrm{g}). \quad (31)$$

According to Krupke's approximation,[13]

$$\sum_{n'} \overline{r^{t+1}}(4,\mathrm{f},n',\mathrm{g}) = \frac{\langle 4\mathrm{f}|r^{t+1}|4\mathrm{f}\rangle}{\Delta(n'\mathrm{g})}. \quad (32)$$

In Krupke's table,[11] $\langle 4\mathrm{f}|r|5\mathrm{d}\rangle$, $\langle 4\mathrm{f}|r^3|5\mathrm{d}\rangle$, $\langle 4\mathrm{f}|r^5|5\mathrm{d}\rangle$, $\langle 4\mathrm{f}|r^4|4\mathrm{f}\rangle$, $\langle 4\mathrm{f}|r^6|4\mathrm{f}\rangle$, $\langle 4\mathrm{f}|r^8|4\mathrm{f}\rangle$, $\Delta(5\mathrm{d})$ and $\Delta(n'\mathrm{g})$ are listed for Pr^{3+}, Nd^{3+}, Eu^{3+}, Tb^{3+}, Er^{3+} and Tm^{3+}. In oxide compounds, $\Delta(5\mathrm{d})$ can be estimated by the work of Dorenbos.[14] Goldner *et al.*[15] give estimations of $\Delta(5\mathrm{d})$ and $\Delta(5\mathrm{g})$ for Yb^{3+}, which are 21700 cm^{-1}, 51340–72340 cm^{-1}, respectively. The radial integrals and energy denominators $\Delta(5\mathrm{d})$ and $\Delta(5\mathrm{g})$ for Tm^{3+} and Eu^{3+} are also listed in Krupke's work.[16]

Based on these works, the values of $\langle 4\mathrm{f}|r^t|5\mathrm{d}\rangle$ and $\langle 4\mathrm{f}|r^{t+1}|4\mathrm{f}\rangle$ used to estimate the values of $\Xi(t,k)$ are shown in Table 1.

Table 1. Estimated radial integrals in atomic units and energy denominators in cm^{-1} of Yb^{3+} for $\Xi(t,k)$ in atomic units.

$\langle 4\mathrm{f}\|r\|5\mathrm{d}\rangle$	0.583	$\langle 4\mathrm{f}\|r^2\|5\mathrm{d}\rangle$	0.6522
$\langle 4\mathrm{f}\|r^3\|5\mathrm{d}\rangle$	2.46	$\langle 4\mathrm{f}\|r^4\|5\mathrm{d}\rangle$	1.57
$\langle 4\mathrm{f}\|r^5\|5\mathrm{d}\rangle$	16.5	$\langle 4\mathrm{f}\|r^6\|5\mathrm{d}\rangle$	7.31
$\langle 4\mathrm{f}\|r^7\|5\mathrm{d}\rangle$	20	$\langle 4\mathrm{f}\|r^8\|5\mathrm{d}\rangle$	62
$\Delta(5\mathrm{d})$	–72340	$\Delta(5\mathrm{g})$	–217000

In the site symmetry C_2, there are twenty-five non-vanishing parameters A^k_{tp}, which are $(k,t,p) = (0,1,0)$, $(2,1,0)$, $(2,3,2)$, $(4,3,2)$, $(2,3,0)$, $(4,3,0)$, $(2,3,-2)$, $(4,3,-2)$, $(4,5,4)$, $(6,5,4)$, $(4,5,2)$, $(6,5,2)$, $(4,5,0)$, $(6,5,0)$, $(4,5,-2)$, $(6,5,-2)$, $(4,5,-4)$, $(6,5,-4)$, $(6,7,6)$, $(6,7,4)$, $(6,7,2)$ $(6,7,0)$, $(6,7,-2)$, $(6,7,-4)$, and $(6,7,-6)$. The values of A^k_{tp} with $p=0$ are real, the others are complex. There are twenty-five independent real parameters. The imaginary and real parts of A^k_{tp} with $p>0$ and A^k_{tp} with $p=0$ were chosen as the independent variables to be fitted. The estimated initial values are shown in Table 2.

Table 2. Initial and fitted parameters of A^k_{tp} with $p \geq 0$, Huang–Rhys factors, and FWHM (in nm).

k,t,p	Initial values/10^{-13} m	Fitted values/10^{-13}m
2,1,0	–0.140	–3.46
2,3,2	–0.001–0.013i	0.26+2.07i
4,3,2	–0.001–0.014i	–3.19−6.06i
2,3,0	0.006	0.83
4,3,0	0.007	0.76
4,5,4	–0.00023–0.0049i	0.42+2.22i
6,5,4	–0.00063-0.013i	7.56+2.56i
4,5,2	–0.0022–0.00918i	3.02–0.91i
6,5,2	–0.0058–0.02492i	6.73+8.74i
4,5,0	–0.05927	–0.38
6,5,0	–0.160853	4.40
6,7,6	0.0007+0.00021i	–6.14–4.57i
6,7,4	–0.0027–0.0012i	–2.29–0.98i
6,7,2	0.00013–0.00032i	3.66–6.32i
6,7,0	–0.001393	–1.44
s_1	0.46	0.414
s_2	0.11	0.055
s_3	0.22	0.185
w_1	2.31515	2.3133
w_2	2.05448	2.1006
w_3	2.18299	2.2250

3.3.2. Fitting intensity and discussion of results

The energy levels of Yb^{3+}:$GdTaO_4$ are shown in Fig. 3. Due to the strong re-absorption, it is very difficult to obtain the accurate line intensity at about 973 nm from the transition $E_5 \rightarrow E_1$, and this line would not be included in our full-profile fitting. On the other hand, the line of 973 nm is a zero-phonon line, on which no obvious phonon vibronic peak was observed, so it is reasonable that no phonon assisted transition was incorporated in the transition $E_5 \rightarrow E_1$, whose electric dipole and magnetic transition probability can be calculated with A^k_{tp} and wavefunctions of Yb^{3+}in $GdTaO_4$, and the calculated energy lifetime of E_5 can be obtained. Correspondingly, the experimental photoluminescence decaytime of 1014 nm and excitation wavelength 972 nm at temperature 8 K was taken as the energy lifetime of E_5, so it is viable to take the energy lifetime of E_5 as a fitted quantity in Eq. (20).

The lattice relaxation shifted the emission wavelength by 5.3 cm^{-1}, so the energy level position of 10285 cm^{-1} was changed and fixed as 10280 cm^{-1} during the fitting procedure in order to keep the calculated transition wavelength consistent with the corresponding experimental line peaks. The vibronic peaks 1009.2 nm, 1020.0 nm, and 1038.6 nm were accounted for, their frequency center shifts are 88 cm^{-1}, 59 cm^{-1}, and 45 cm^{-1} relative to the electronic state transition peaks 999.8 nm, 1013.4 nm, and 1033.3 nm, and were approximated by single-frequency phonons here, whose Huang–Rhys factors labeled by S_1, S_2, and S_3 were also fitted. On the other hand, the FWHM of the lines of 1000.3 nm, 1014 nm, and 1033 nm peaks with Lorentz profiles, which were labeled as w_1, w_2, and w_3, respectively, were also included in the fitting. In sum, the fitting variable $\boldsymbol{x}$ is composed of twenty-five components of A^k_{tp}, three Huang–Rhys factors S_1, S_2, S_3, and FWHM w_1, w_2, w_3, and σ_I, respectively.

A detailed Levenberg–Marquardt iteration algorithm with Eq. (25) is described in Ref. [17]. Here, the maximal iteration loop number, and searching damping factor loop number were set as 100 and 40, respectively.

The refractive index of Yb^{3+}:$GdTaO_4$, which is necessary for calculating transition probabilities, is calculated by the equation[18]

$$n^2 = A + \frac{B}{\lambda^2 - C} - D\lambda^2, \tag{33}$$

where $A = 3.89546$, $B = 0.53175$ μm^2, $C = -0.30491$ μm^2, and $D = -0.05039$ μm^{-2}.

After 88 iterations, the relative residual R is 11.75%, and the experimental and fitting curves are shown in Fig. 4. The calculated energy lifetime is 363.99 μs, which is close to the experimental value 364 μs. The fitted curves are very consistent with the experimental curves. The fitted A^k_{tp} values are shown in Table 2. Comparing the fitted A^k_{tp} with their initial values, the difference between the initial and fitted values is large, but the initial and final values of $(k,t,p) = (2,1,0)$, $(4,3,2)$, $(2,3,0)$, $(4,3,0)$, $(4,5,0)$, $(6,7,4)$, $(6,7,2)$, and $(6,7,0)$ keep the same sign.

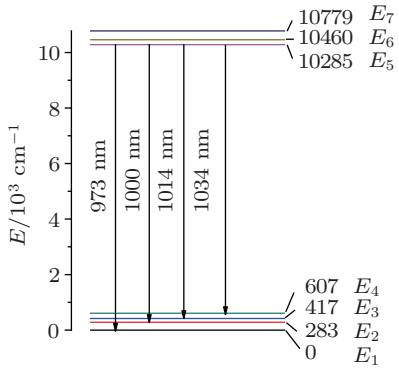


Fig. 3. Energy levels of Yb^{3+}:$GdTaO_4$.

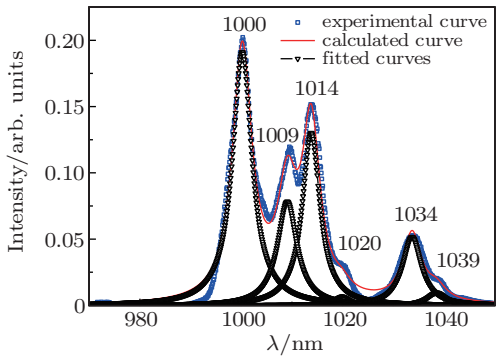


Fig. 4. The experimental and calculated photoluminescence curves of Yb:$GdTaO_4$.

The transition probabilities and line strengths obtained from the intensity fitting are shown in Table 3. It can be seen that the electric dipole transitions are dominant, the main component of magnetic dipole transition is the transition $E_5 \rightarrow E_1$, whose ratio to electric dipole is 31%, $E_5 \rightarrow E_4$ and $E_5 \rightarrow E_4$+phonon is 0.3%, while the others are far less than 1%. The fluorescence branch ratios are also listed in Table 4. The highest branch ratio, 39.5% is from the transition $E_5 \rightarrow E_2$, and the second is $E_5 \rightarrow E_3$, whose branch ratio is 24.7%. The emission cross section of $E_5 \rightarrow E_1$ is calculated with the obtained A_{tp}^k and the Lorenz profile with FWHM 1.33 nm of 973 nm, and the other transitions $E_5 \rightarrow E_2, E_3, E_4$ have also been calculated, and their curves are shown in Fig. 5. The emission cross sections of 973 nm, 1000 nm, 1009 nm, 1014 nm, 1019 nm, 1034 nm, 1039 nm are 2.1, 10.0, 6.0, 8.2, 1.8, 3.4, and 1.3 in 10^{-20} cm^2, respectively. From Fig. 1(b), we can see that the experimental intensity of $E_5 \rightarrow E_1$ is very weak at 8 K temperature, which is the result of reabsorption. As a comparison, the emission cross section of Yb^{3+}:$GdTaO_4$ was calculated by the F–L equation[19]

$$\sigma_{\rm em} = \frac{\lambda^2 g(\nu)}{8\pi n^2 \tau_{\rm rad}} = \frac{\lambda^4 g(\lambda)}{8\pi c n \tau_{\rm rad}}. \tag{34}$$

The emission cross sections obtained by this equation are also shown in Fig. 5. The emission cross sections of 973 nm, 1000 nm, 1009 nm, 1014 nm, 1019 nm, 1034 nm, 1039 nm are 2.6, 11.1, 6.8, 8.8, 2.0, 3.4, and 1.3 in 10^{-20} cm^2. It can be seen that the emission cross sections obtained by F–L in the low wavelength range are less than the calculated values, which maybe results from the case that $g(\lambda)$ is smaller than the value when there is reabsorption. The relative error ratios of the emission cross sections given by the F–L formula to calculated values by full-profile method are 23%, 11%, 13%, 7%, and 11% at the wavelength 973 nm, 1000 nm, 1009 nm, 1014 nm, and 1019 nm, respectively. This indicates that the emission cross sections obtained by the F–L formula are higher than the actual values in the low wavelength region and, otherwise, are the same as that in the long wavelength range.

Table 3. The transition probabilities and line strengths of Yb^{3+}:$GdTaO_4$.

Transition	λ/nm	$A_{\rm ed}$/s^{-1}	$S_{\rm ed}$/10^{-20} cm^2	$A_{\rm md}$/s^{-1}	$S_{\rm md}$/10^{-23} cm^2	A/s^{-1}	Branch ratio%
$E_5 \rightarrow E_1$	973	115.7	0.032	35.6	10.2	151.3	5.5
$E_5 \rightarrow E_2$	1000	1083.2	0.33	1.5	0.5	1084.7	39.5
$E_5 \rightarrow E_2$+phonon	1009	447.6	0.14	0.6	0.2	448.2	16.3
$E_5 \rightarrow E_3$	1014	674.2	0.22	5.5	1.8	679.7	24.7
$E_5 \rightarrow E_3$+phonon	1019	37.3	0.01	0.30	0.1	37.6	1.4
$E_5 \rightarrow E_4$	1034	290.4	0.1	0.9	0.3	291.3	10.6
$E_5 \rightarrow E_4$+phonon	1039	54.3	0.019	0.2	0.06	54.5	2.0

Table 4. Thermal populations (%) of E_1–E_4 of Yb^{3+}:$GdTaO_4$.

T/K	Thermal population/%			
	E_1/0 cm^{-1}	E_2/283 cm^{-1}	E_3/417 cm^{-1}	E_4/607 cm^{-1}
8	100	0	0	0
100	98.1	1.7	0.2	0
200	83.8	10.9	4.2	1.1
300	69.1	17.8	9.4	3.8

Although the transition intensity parameters A_{tp}^k have been obtained, Judd–Ofelt transition intensity theory with the triplet parameters Ω_t $(t = 2, 4, 6)$ cannot be applied at low temperatures because the populations in the stark levels of $^2F_{7/2}$ or $^2F_{5/2}$ are unequal. It can be seen that the photoluminescence of Yb^{3+} in $GdTaO_4$ at 8 K are from the lowest stark level E_5 of $^2F_{5/2}$, and the transitions from the other stark levels of $^2F_{5/2}$ were not observed. So the approximation that the photoluminescence is caused by the multiple transitions of $^2F_{5/2} \rightarrow {}^2F_{7/2}$ is not valid, which can be shown as follows. The Ω_t $(t = 2, 4, 6)$ calculated with the parameters A_{tp}^k are 0.27, 1.46, 6.67 in 10^{-20} cm^2. The electric dipole transition line strength can be calculated by

$$S_{\rm ed}|^2F_{5/2}\rangle \rightarrow |^2F_{7/2}\rangle = \sum_{t=2,4,6} \Omega_t \left(\langle {}^2F_{7/2}||U^t||{}^2F_{5/2}\rangle\right)^2, \tag{35}$$

in which the values of $(\langle {}^2F_{7/2}||U^t||{}^2F_{5/2}\rangle)$ $(t = 2, 4, 6)$ are $\sqrt{6}/7$, $2\sqrt{5}/7$, and $\sqrt{6/7}$. The calculated $S_{\rm ed}$ is 7.2×10^{-20} cm^2, which is much greater than the 0.86×10^{-20} cm^2 obtained from fitting to the emission spectrum of Yb^{3+}:$GdTaO_4$. Apart from the unequal Boltzmann population of the stark levels of $F_{5/2}$, the relaxation from the higher stark levels to the lowest stark level E_5 of $^2F_{5/2}$ in Yb^{3+}:$GdTaO_4$ results in a more unequal population. So only the transitions from the lowest stark level of $^2F_{5/2}$ to the stark levels of $^2F_{7/2}$ were observed experimentally.

When Yb^{3+}:$GdTaO_4$ is used as a laser medium, it is expected that laser operation at the zero-phonon line 972 nm is not realizable due to strong reabsorption. If the laser operates as follows: Yb^{3+} is pumped to the excited level E_6, rapidly relaxed to E_5, and then transitions to the background state E_1, a three-level system forms, and a very high laser threshold is expected, so the optical transition of $E_5 \rightarrow E_1$ is non-

sense for laser operation. It can be seen that the emission cross sections in the range of 1000–1019 nm from $E_5 \rightarrow E_2$, E_3 are high, and no great reabsorption occurs at low temperatures, the prospect of realizing laser operation in this channel is promising. When the working temperature of laser material increases, the thermal population of E_2 increases, and the reabsorption of 1000 nm increases, which result in the case that the strongest line is 1014 nm, rather than 1000 nm at room temperature, which is shown as Fig. 6. Table 4 lists the thermal populations of E_1–E_4 at 8 K, 100 K, 200 K, and 300 K. It can be seen that the population of the lowest level E_1 decreases, while the populations of the other levels increase gradually with increasing temperature. High thermal population of E_2–E_4 will result in difficulty of laser population inversion, so it is desirable for Yb^{3+}:$GdTaO_4$ to operate at a low temperature.

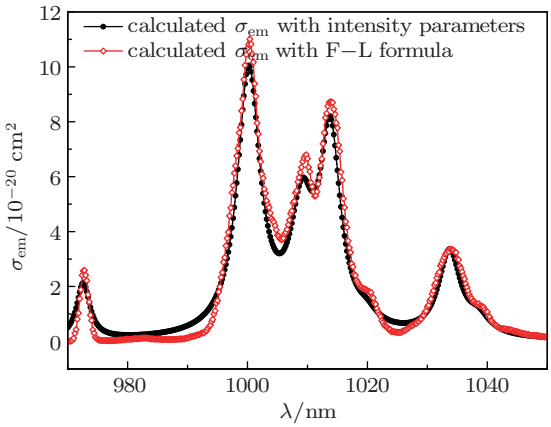


Fig. 5. Emission cross sections of Yb^{3+}:$GdTaO_4$ calculated with the F–L formula and intensity parameters fitted.

At the same time, an increase in host temperature also results in broadening the FWHM of the emission spectrum, and a continuous emission band from 1001 nm to 1035 nm can be observed at room temperature (shown in Fig. 6) due to a remarkable increase in the strong phonon assist. The bandwidth of 34 nm is nearly equal to gain bandwidth $\Delta\nu_0^*$ 10.2 THz. The pulse width $\Delta\tau_p$ of a mode-locked laser can be estimated by[20]

$$\Delta\tau_p \cong \frac{0.441}{\Delta\nu_0^*}, \tag{36}$$

where $\Delta\nu_0^*$ is gain bandwidth, which gives $\Delta\tau_p \cong 43$ fs and favors the femtosecond pulse width. The E_6, as the pump level of a 970 nm laser diode (LD), E_5, as a laser up level, and E_2, E_3, E_4 as the terminal levels, of Yb^{3+}:$GdTaO_4$ form a good quasi-four-level system of femtosecond laser or tuning laser from 1000–1034 nm. High power laser diodes of 970 nm are commercially available at good prices, so Yb^{3+}:$GdTaO_4$ is a very promising laser material with the wide tuning laser wavelength of 1000–1034 nm or a ultra-short pulse laser pumped by LD, which can be used in many fields such as machining, gas detection, and so on.

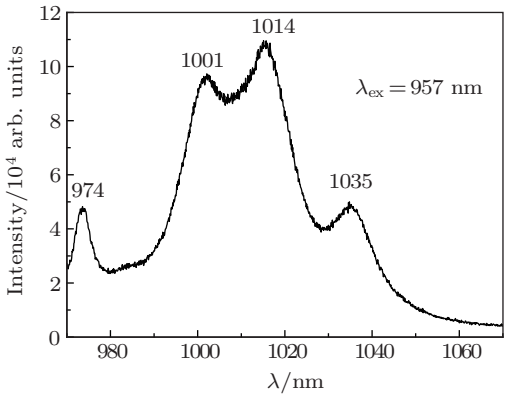


Fig. 6. Emission spectrum of Yb^{3+}:$GdTaO_4$ with excitation wavelength 930 nm.

4. Conclusion

Full profile fitting to the emission spectrum of rare-earth ions in solids to obtain transition intensity parameters was proposed, in which the contribution of a transition to the emission spectrum is expressed as the product of transition probability, line profile function, instrument measurement constant and transition center frequency or wavelength, and the whole emission spectrum is the sum of the transitions. Then the emission spectrum is expressed as a function with independent variables intensity parameters A_{tp}^k, full width at FWHM of profile functions, instrumental constant, wavelength, Huang–Rhys factor S if lattice vibronic peaks in the emission should be considered and so on. Meanwhile, quantities of the energy lifetime are incorporated into the fitting function to remove the arbitrariness of determining the intensities A_{tp}^k and other parameters. Employing this method, makes measuring the absolute emission spectrum intensity unnecessary and does not depend on the number of emission transition peak intensities. Every experimental data point in the emission spectrum, usually hundreds or more, is the function with intensity parameters A_{tp}^k as variables, so it is usually viable to determine A_{tp}^k with a large number of experimental data points. Twenty-five A_{tp}^k of Yb^{3+} in $GdTaO_4$ were determined by this method. The calculated and experimental energy lifetimes, emission spectrum are very consistent, indicating that it is viable to obtain the transition intensity parameters of rare-earth ions in solids by full profile fitting. The calculated emission cross sections of Yb^{3+}:$GdTaO_4$ also indicate that the F–L formula gives higher values at the low wavelength range. $GdTaO_4$ has a strong phonon assisted transition even at low temperature, as shown by Huang–Rhys factors 0.414, 0.055, and 0.185 of $E_5 \rightarrow E_{4,3,2}$, which result in a broad emission band from 1000–1019 nm at low temperature, and 1000–1034 nm at room temperature. This makes it a very promising tuning and ultra-short-pulse laser material when pumped by an LD of 970 nm.

References

[1] Judd B R 1962 *Phys. Rev.* **127** 750
[2] Ofelt G S 1962 *J. Chem. Phys.* **37** 511
[3] Reid M F and Richardson F S 1984 *J. Chem. Phys.* **88** 3579
[4] Newman D J and Balasubramanian G 1975 *J. Phys. C: Solid State Phys.* **8** 37
[5] Reid M F and Richardson F S 1983 *J. Chem. Phys.* **79** 5735
[6] Reid M F, Dallara J J and Richardson F S 1983 *J. Chem. Phys.* **79** 5743
[7] Newman D J and Ng B 2000 *Crystal Field Handbook* (New York: Cambdrige Univeristy Press) p. 208
[8] Judd B R 1963 *Operator Techniques and Atomic Spectroscopy* (New York, San Francisco, Toronto, London: McGraw-Hill Book Company) p. 42, p. 72
[9] Theo H 2005 *International Tables for Crystallography, Volume A: Space-Group Symmetry* (5th edn.) (Dordrecht: Springer) p. 195
[10] Huang K 1981 *Adv. Phys.* **1** 31
[11] Zhang Q L, Wang X M, Yin S T and Jiang H H 2008 *Eng. Sci.* **10** 35
[12] Zhang Q L, Ning K J, Ding L H, Liu W P, Sun D L, Jiang H H and Yin S T 2013 *Chin. Phys. B* **22** 067105
[13] Krupke W F 1966 *Phys. Rev.* **145** 325
[14] Dorenbos P 2000 *J. Luminun.* **91** 155
[15] Goldner P, Schaudel B and Prassas M 2002 *Phys. Rev. B* **65** 054103
[16] Krupke W F and Gruber J B 1965 *Phys. Rev. B* **139** A2008
[17] Ma Z 2005 *Handbook of Modern Applied Mathematics, Computational and Numerical Analysis* (Beijing: Tsinghua University press) p. 554
[18] Liu W 2009 *Preparation, Single Crystal Growth and Luminescence Properties of New Type Scintillators with High Density* (Hefei: Ph D Dissertation of Chinese Academy of Sciences) p. 92
[19] Patel F D, Honea E C, Speth J, Payne S A, Hutcheson R and Equall R 2001 *IEEE J. Quantum Electron.* **37** 135
[20] Orazio S 1998 *Principles of Lasers* (4th edn.) (New York and London: Plenum Press) p. 339